CHAPTER–6

A New 3-fold Interpenetrated Zn(II)-Metal-Organic-Framework of Bis(pyridyl)-phenylene-di-imine: Application as Catalyst in Knoevenagel Condensation

A New 3-fold Interpenetrated Zn(II)-Metal-Organic-Framework of Bis(pyridyl)-phenylene-di-imine: Application as Catalyst in Knoevenagel Condensation

6.1 Introduction

Porosity being one of the desired properties of MOFs, which can be achieved by adopting various crystal engineering techniques including tuning of ligands, metal nodes, and reaction conditions. Porous MOFs has a wide range of potential applications in gas storage/sequestration, catalysis, drug delivery, etc.[1] Advantageous structural features in MOFs, such as tunable pore sizes, high pore volume, surface area and cavity functionality, which can be tailormade to cater the need of the application, makes them most suitable candidates for catalysis. The presence of uniform and continuous channels in porous MOFs help in facilitating the transport of substrates while metal center/metal clusters and various ligand functionalities can act as active sites for the substrate binding. The possibility of attaining a wide range of porosity in MOFs makes them suitable catalyst[2] for substrates ranging from small molecules to large polyaromatics and carbohydrates. The application of MOFs in catalysis was explored by many leading research groups in the last two decades.[3] Among the various organic reactions, MOFs were exploited as a catalyst for Knoevenagel condensation,[4] Henry reaction,[5] transesterification,[6] alkene oxidation,[7] alcohol oxidation,[8] olefine epoxidation,[9] epoxide ring opening,[10] cyanosilylation,[11] Friedel-Craft alkylation (MOF-5),[12] Ullman-coupling reaction (MOF-199),[13] NO_2 reduction (Zr-MOF),[14] aminocarbonylation (MOF-5),[15] hydrolysis of ammonia borane.[16]

Park et al., have reported a multifunctional 3D interpenetrated porous coordination network (PCN-124), which catalyzed the one-pot tandem reaction, wherein de-acetalysation is promoted by acidic Cu(II) ion and Knoevenagel condensation was activated by Lewis basic site of pyridine and amide groups.[17] Fujita et al., have reported a Cd(II) coordination polymer of 4,4′-bipyridine that catalyzed the cyanosilylation of aldehyde to give 77% yield.[18] Alaerts et al., have studied the catalytic property of the MOF **HKUST**, $Cu_3(btc)_2$, in which a large cavity of pore volume 0.6-0.65 $cm^3\ g^{-1}$ and open metal site resulted due to the desolvation provided the Lewis acid site which facilitated the cyanosilylation benzaldehyde and ketone.[19] Kantan group has explored the catalytic properties of Cu-MOFs of di/tri-carboxylic acids in hydroxylation and nitration of aryl halides.[20] **MIL-47** and **MOF-48** were explored as catalysts by Yaghi et al., for the conversion of methane to acetic acid. Both these MOFs are isostructural and constructed by benzene-1,4-dicarboxylate and 2,5-dimethyl- benzene -1,4-dicarboxylate, respectively, with vanadium as the metal center. Hydrophobic pores of **MOF-48** and vanadium

metal center act as an active catalytic site for this conversation.[21] Hartmann[22] and Gascon[23] have investigated the catalytic active species of the amino group in different MOFs including '**IRMOF**', '**MIL-101**(Fe)', etc., for base-catalyzed Knoevenagel condensation. Kaskel et al., have synthesized a Zn-MOF, wherein homo chiral 18 × 18 $Å^2$ rectangular channel were effectively utilized in asymmetric reaction.[24] **IRMOF-3**, **MIL-53**, **Fe-MIL-101-NH_2**, **Al-MIL-101-NH_2**, **CAU-1**, **UiO-66-NH_2**, **MOF-5**, **MIL-53** (Al) are effectively used as the catalyst for Knoevenagel condensation with a product yield up to 90%–95% within 2-3 hours, wherein the most of them are designed by mixed dicarboxylate linkers.[22-23, 25]

Catalysis by MOFs can be categorized according to the reaction mechanism and functionalities present in MOFs as (i) Lewis acid catalysis, (ii) base catalysis, and (iii) bifunctional acid-base catalysis.[4, 26] There are very few reports on base catalysis due to the difficulties involved in synthesizing free nitrogen-containing MOF.[27] Post-synthetic modification has effectively resulted in incorporating various functionalities in MOFs which in turn affected the catalytic efficiencies.[28] Post-synthetically grafting of amine spacers in **MIL-101**(Cr) and incorporating 3-aminopropylsilane on Lewis acidic site of the MOF resulted in the superior basic catalytic activity in the Knoevenagel condensation.[29] Encapsulation of polyoxometalate into the MOF also showed an increase in catalytic efficiency.[30] Coordination polymers (CPs)[31] where acidic sites are available to have shown efficient catalysis in Knoevenagel condensation. Commercially available Basolite C300 Cu-MOF has shown better catalytic activity in Knoevenagel condensation than that of zeolites.[32]

Schiff base oriented MOF catalyst sewed with dicarboxylate ligand also generated an active catalytic site for many organic reactions.[33] Mechanochemically synthesis of Zn-MOF of **TMU-4**, **TMU-5**, and **TMU-6** have been constructed from bis(pyridyl)-di-imine and a non-linear 4,4′-oxybisbenzoic acid resulted in good catalytic activity in Knoevenagel condensation.[34] Among them, **TMU-5** has shown the best result due to its narrow-interconnected pore size of 4.4 Å × 6.2 Å and azine group of imine functionality. Further, these three MOFs have synthesized in coordination modulation method by introducing capping agent to produce micro and nano shaped MOF with rod and plate-like morphology.[35]

General requirements in MOFs to act as potential catalyst include (1) Active metal center and active functional group in organic ligands, (2) Coordinatively unsaturated metal center, (3) Incorporating non-covalent synthon into organic ligands, (4) Controllable pore size by using flexible organic ligands, (5) Accessible pores by removing guest molecules. In this chapter, a

new 3D plate-like morphology of **Zn(II)-MOF** is designed by using linear 4,4′-dicarboxylic acid (**4,4′-bp**) and imine functionalized bis(pyridyl)-phenylene-di-imine (**L14c)** ligands. The presence of Zn(II) center can serve as Lewis acid sites while imine ligand can act as a basic site in the MOF, which can be driving factor involved in the catalysis of various condensation reactions. Herein, catalysis of Knoevenagel condensation reaction is studied for **Zn(II)-MOF**, where benzaldehyde and its derivatives were treated with the active methylene compound malononitrile in methanolic solution.

6.2 Experimental

6.2.1 General

^{1}H and ^{13}C spectra were recorded on a 400 MHZ spectrophotometer (Bruker). IR spectra were taken from Shimadzu model-00247 IRAffinity-1S. Thermogravimetric analysis performed by using Shimadzu TGA-50 with the flowing rate of N_2 is 10 °C/min. Powder X-Ray Diffraction (XRD) was recorded with a Rigaku miniflex II, λ =1.54 Å, Cu Kα. Solid-state UV-Visible Spectra were obtained using Shimadzu spectrophotometer. 4-pyridinecarboxaldehyde and 4,4′-biphenyl were purchased from Sigma Aldrich. All other chemicals like *p*-phenylenediamine, $Zn(NO_3)_2.6H_2O$, and solvents were purchased from local vendors and used further without purification. GC was carried by Shimadzu GC-2014 with FID detector.

6.2.2 Synthesis of (1E,1'E)-*N*,*N*'-(1,4-phenylene)bis(1-(pyridin-4-yl)methanimine) (L14c)

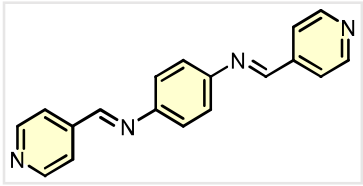

p-Phenylenediamine (0.270 g, 2.5 mmol) was added dropwise to a methanolic solution of 4-pyridinecarboxaldehyde (0.716 g, 5 mmol). The mixture was kept for 4 hours at 60 ˚C under refluxing condition. Yellow precipitate was removed by filtration and washed with hexane and finally recrystallized with methanol. Yield: 72%; melting point: 204.5 ˚C; IR (cm^{-1}): 1633 (m), 1619 (m), 1599 (m), 1678 (m), 1551 (m), 1508 (w), 1486 (m), 1412 (m), 1324 (m), 1191(m), 1160 (m), 1099 (m), 989 (w), 888 (m), 835 (s), 812 (s), 795 (m), 604 (m), 565 (m), 525 (m). (Figure A-134). ^{1}H NMR (400 MHz, DMSO-d_6) δ ppm: 8.80 (d, *J* = 6.0 Hz, 2H), 8.74 (d, *J* = 6.0 Hz, 2H), 8.54 (s, 1H), 8.51 (s, 1H), 7.80 (d, *J* = 6.0 Hz, 2H), 7.75 (d, *J* = 6.0 Hz, 2H), 7.37 (s, 2H), 7.24 (d, *J* = 6.6 Hz, 1H), 6.75 (d, *J* = 8.7 Hz, 1H) (Figure A-135).

6.2.3 Synthesis of Zn(II)-MOF $[C_{62}\ H_{38}\ N_4O_{14}Zn_3]_n$

L14c, [1,1′-biphenyl]-4,4′-dicarboxylic acid, and $Zn(NO_3)_2.6H_2O$ were taken in 1:4:4 ratio and hand grinded using mortar-pestle. The yellow dry powder after grinding for 15 minutes turned into a soggy chocolate color. Then 15 ml of DMF was added and transferred into teflon vessel and finally kept in an autoclave at temperature 120 ˚C and pressure 30 bar for 2 days. After 2 days, the temperature was decreased at a rate of 10 ˚C/hour. Yellow block-shaped crystals were collected (Crystal data is given in Table 6.1). Yield: 90%, IR (cm^{-1}): 1670 (m), 1599 (m), 1541 (w), 1377 (s), 1211(w), 1176 (w), 1091 (m), 1080 (w), 1023 (w), 838 (m), 768 (s), 677 (m), 459 (m) (Figure A-136).

Table 6.1: Crystal data of Zn(II)-MOF

Parameters	**Zn(II)-MOF**
Chemical formula	$C_{62}\ H_{38}\ N_4O_{14}Zn_3$
Formula weight	1259.13
Temperature (K)	297(2)
Wavelength (Å)	0.71073
Crystal system	Monoclinic
Space group	*P* $2_1/n$
a (Å)	11.5156(12)
b (Å)	14.7449(15)
c (Å)	19.327(2)
α (°)	90
β (°)	102.805(5)
γ (°)	90
Z	2
Volume ($Å^3$)	3200.0(6)
Density (g/cm^3)	1.307
μ (mm^{-1})	1.178
Theta range	2.967° to 25.000°
F(000)	2080
Reflections collected	35491
Independent reflection	5454
Reflections with I >2σ(I)	3834
R_{int}	0.1033
Number of parameters	392
GO F on F^2	1.035
Final $R_1{}^a/wR_2{}^b$ (I >2σ(I))	0.0889/0.2063
Largest diff. peak and hole ($eÅ^{-3}$)	0.850/-0.864

[a] $R_1 = \sum||F_o| - |F_c||/\sum|F_o|$. [b] $wR_2 = [\sum w(F_o^2 - F_c^2)^2/\sum w(F_o^2)^2]^{1/2}$,

where $w = 1/[\sigma^2(F_o^2) + (aP)^2 + bP]$, $P = (F_o^2 + 2F_c^2)/3$

6.3 Results and discussion

6.3.1 Crystal structure analysis of Zn(II)-MOF

Crystal structure analysis of **Zn(II)-MOF** showed that it has crystallized in a monoclinic space group $P2_1/n$ with four 2-fold axes through the two glide planes. The presence of carboxylate groups in **4,4′-bp** ligands has resulted in the formation of a trinuclear metal cluster with Zn(II) center in **Zn(II)-MOF**. The cluster can be described in terms of pinwheel structure (Figure 6.2a & 6.3). The geometry of two outer Zn(II) in the cluster are tetrahedral while the central Zn(II) being octahedral and resides at a crystallographic $\bar{3}$ site with larger Zn–O bond distance of 2.096 Å than tetrahedral Zn–O bond distance of 1.937 Å. The coordination environment of the outer Zn(II) is being satisfied by carboxylates of three **4,4′-bp** and pyridyl-N of one **L14c** and the coordination environment of the central Zn(II) in the cluster is fulfilled by the carboxylates of six **4,4′-bp** only. The dimeric units octahedral Zn(II) and tetrahedral Zn(II) are connected by the three bifurcated carboxylates anions of **4,4′-bp** and one **L14c** ligand and resulted in a trinuclear $Zn_3(CO)_6N_2$ secondary building units (SBUs) showing a paddlewheel geometry around the Zn-Zn-Zn axis due to the *syn-anti* coordination mode of six **4,4′-bp** (Figure 6.1b). The distance between the two Zn(II) ions in these SBUs is 3.543 Å. Three Zn(II) atoms are propagated in linear geometry lying on a 3-fold axis. The hexagonal pinwheel structure is observed when SBUs units are connected with **4,4′-bp** in the form of a two-dimensional layer with $3^6 \cdot 4^3$ topologies. The 2D layer is further pillared by the **L14c** ligands three-dimensionally and resulted in a formation of hex net with $3^6 \cdot 4^{18} \cdot 5^2 \cdot 6^1$ topologies based on pillar-layered 3D frameworks (Figure 6.2c). Three such hex nets are interpenetrated to each other.

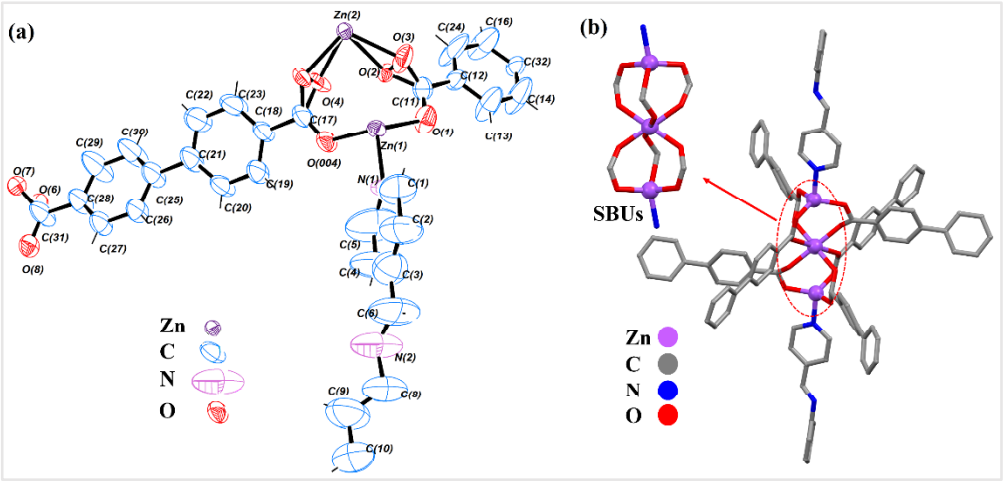

Figure 6.1: (a) ORTEP of asymmetric unit of **Zn(II)-MOF** showing thermal ellipsoids at 50% probability level; (b) Coordination environment of Zn(II) center and the resultant secondary building unit (SBU)

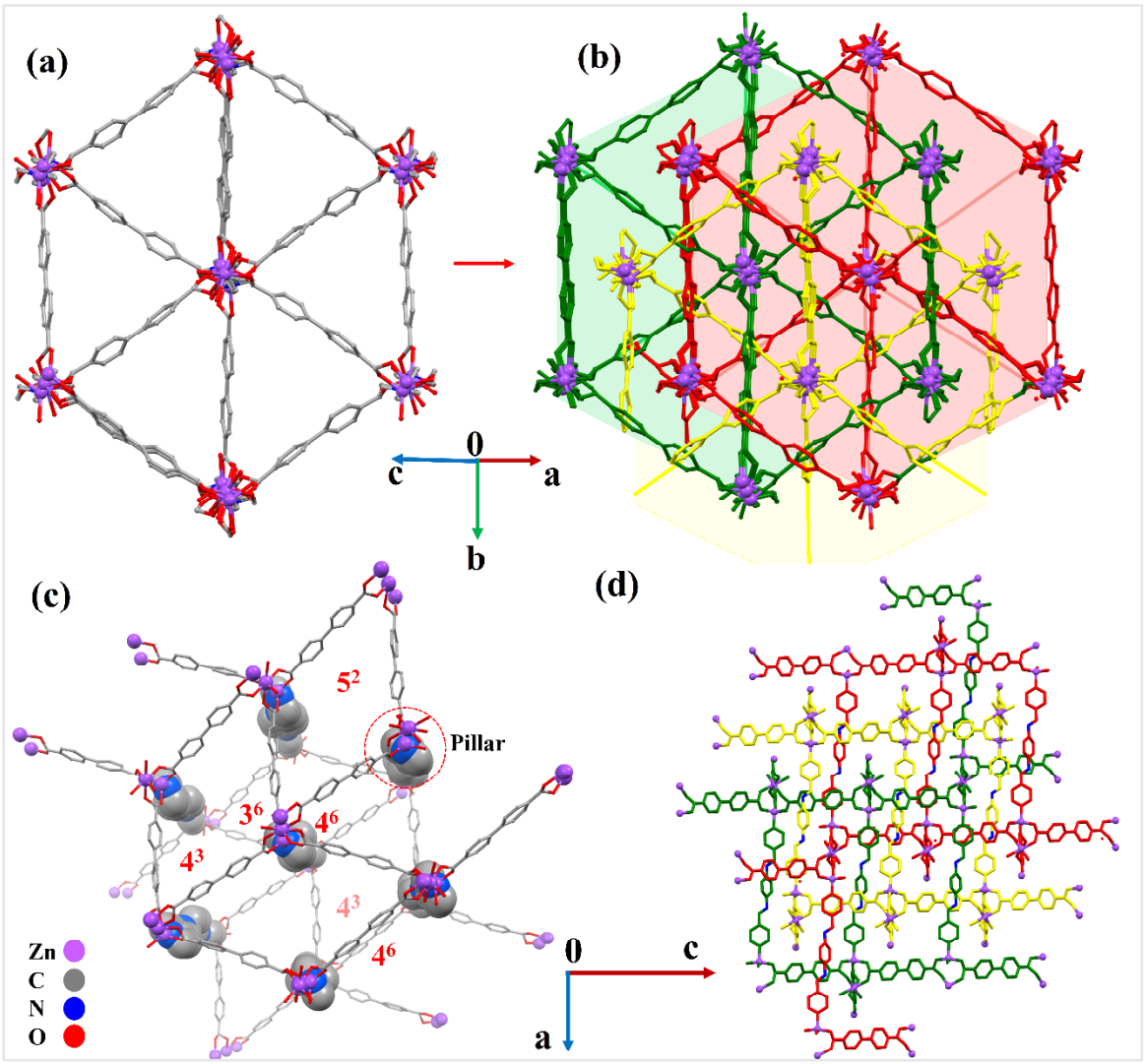

Figure 6.2: Illustrations of crystal structure of **Zn(II)-MOF**: (a) A triangle-tessellated hexagonal net; (b) Interpenetrated 3 hexagonal net; (c) Showing different topologies in one complete pinwheel hex net with pillar; (d) Side view of interpenetrated network in ac plane

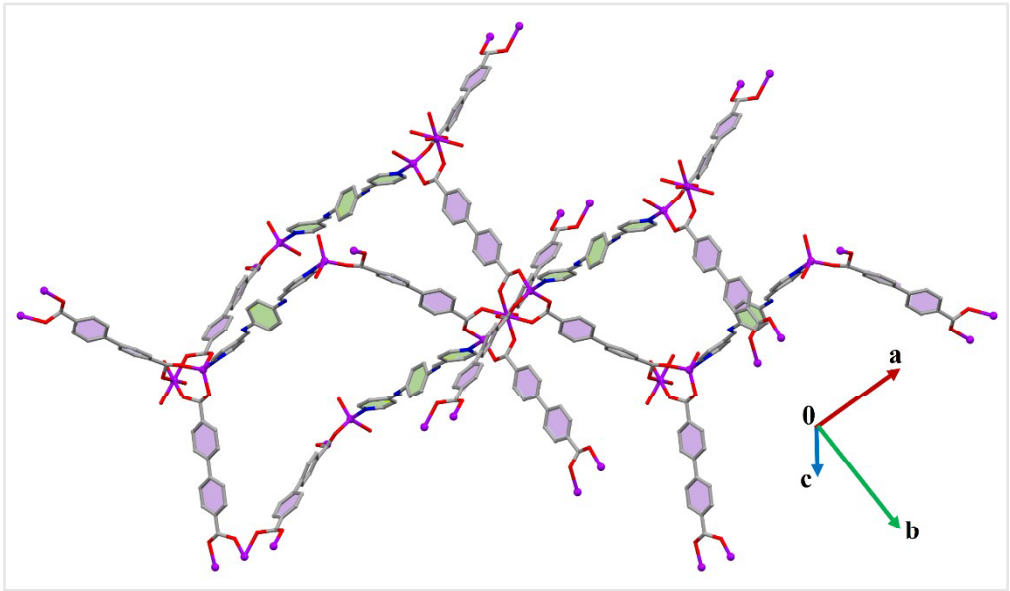

Figure 6.3: Extended the core moiety of **Zn(II)-MOF**

6.3.2 Thermal stability of the Zn-MOF

The thermal stability of **Zn(II)-MOF** was examined by thermogravimetric analysis under a nitrogen atmosphere of 50 ml/min with heating rate 10 °C/min up to 800 °C. The TGA graph in Figure 6.4 represents the two major weight loss at 407.57 °C and 458.71 °C. The derivative curve i.e., the first derivative of weight % with respect to temperature (red line) represents these weight loss %. The molecular weight of **Zn(II)-MOF** is 1259.13 g/mol. 11.347 mg of **Zn(II)-MOF** was taken for analysis. Weight loss 31.1857 % and 32.7932 % are attributed to the decomposition of the MOF frameworks. The **Zn(II)-MOF** is stable above this temperature. 19.6786 % of the weight has remained which corresponds to ZnO.

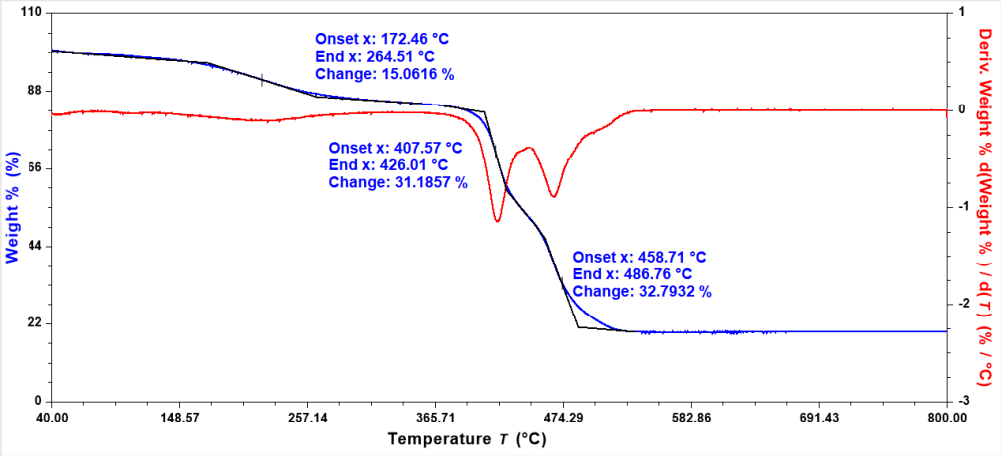

Figure 6.4: Thermogravimetric analysis of the **Zn-MOF**

6.3.3 Water stability of the Zn(II)-MOF

The water stability is very important to analyse the MOF for practical application. The **Zn(II)-MOF** was dipped into the distilled water for 10 hours. The new crystallinity of Zn-MOF was formed after water washing (Figure 6.5b). The phase purity of synthesized Zn-MOF was matched with simulated PXRD spectra which originated from the crystal data (Figure 6.5a).

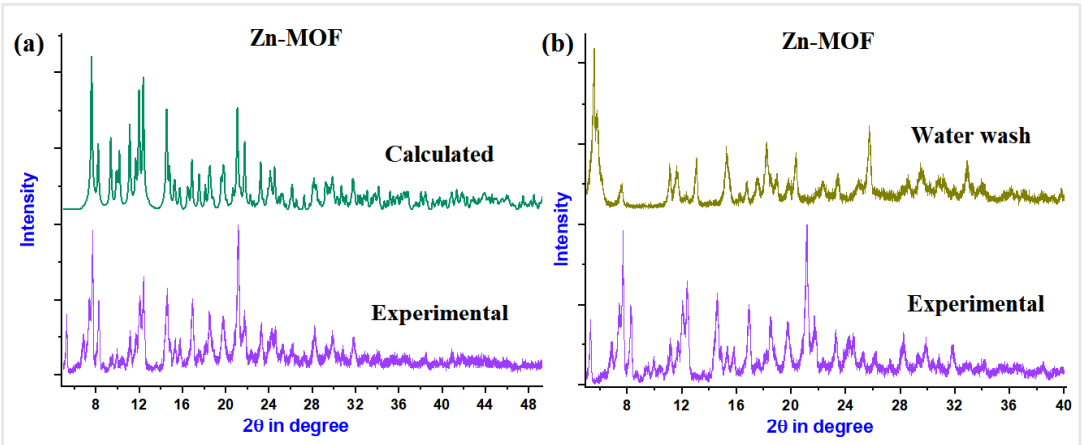

Figure 6.5: (a) Phase purity comparison between calculated PXRD and experimental PXRD of **Zn-MOF**; (b) Represents changing crystallinity after water wash of **Zn-MOF**

6.3.4 Catalytic activity of Zn(II)-MOF

The catalytic activity of **Zn(II)-MOF** was performed in Knoevenagel condensation reaction using methanol as a solvent at 78 °C and the observed results are shown in Table 6.2. Malononitrile was treated with benzaldehyde and refluxed with catalyst (Scheme 6.1). All reactions were monitored by the thin-layer chromatography technique. The product was

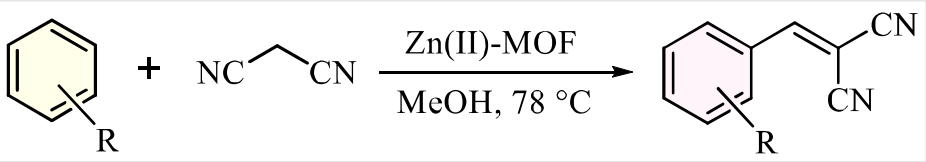

Scheme 6.1: **Zn(II)-MOF** catalysed Knoevenagel condensation between active methylene and aldehyde substrate

Table 6.2: Knoevenagel condensation of benzaldehydes and malononitrile [a]

Reactant 1	Reactant 2	Product	Catalyst amount	Time	Conversion[b] (%)
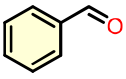	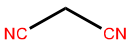	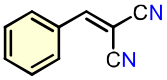	0 mg	24 h	27
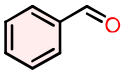	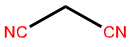	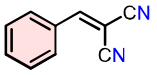	5 mg	30 min	98
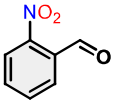	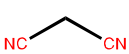	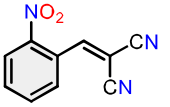	5 mg	30 min	98.2
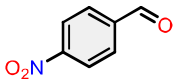	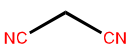	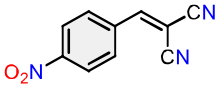	5 mg	30 min	84.3
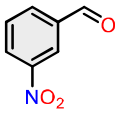	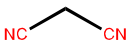	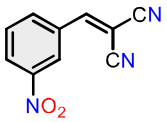	5 mg	30 min	98.2
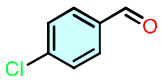	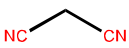	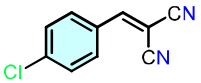	5 mg	30 min	97.8
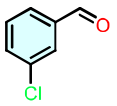	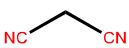	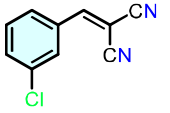	5 mg	30 min	83.3
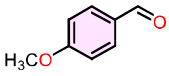	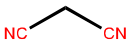	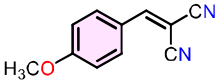	5 mg	45 min	97.4
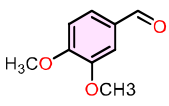	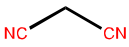	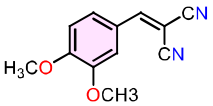	5 mg	45 min	98.5
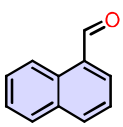	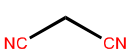	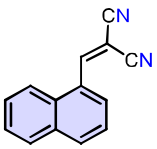	5 mg	30 min	97.9

[a]Reaction performed at 78 °C in methanol, [b]Conversion was determined by GC.

separated by centrifugation and the solvent was evaporated and the residue was scratched by hexane ether solvents. The product was confirmed using ^{1}H NMR spectra analysis (Figure A-137 to A-145). The catalyst was recovered and washed with ethyl acetate. At the end of the reaction, the product conversion was calculated by monitoring the starting material malononitrile of reaction mixture through gas chromatogram apparatus (Carrier gas-nitrogen; flow rate 0.5 ml/min; oven: 190 °C; injector: 250 °C; detector: 250 °C). The reaction was performed with a catalyst and without a catalyst to compare the results. After the catalytic performance of the **Zn(II)-MOF**, powder XRD (Figure A-146) and infra-red spectra were measured to check the structural integrity (Figure 6.6 & 6.7). The possible mechanism was

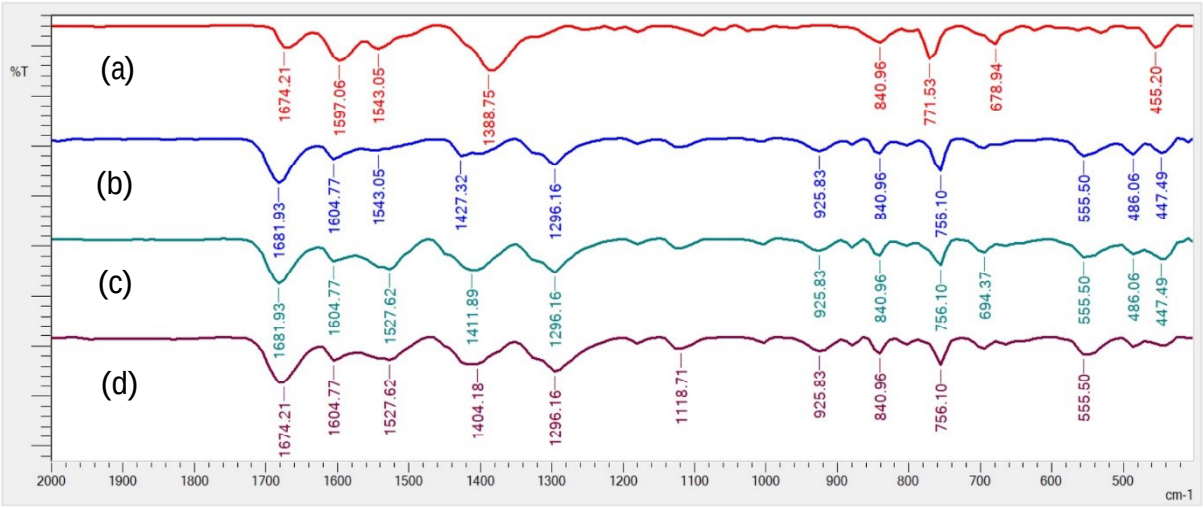

Figure 6.6: Stacked IR spectra compared structural integrity of **Zn(II)-MOF** catalyst (before catalysis) (a) & after catalysis; first cycle (b) second cycle; (c) third cycle

drawn according to literature which shown in Figure 6.8.[36] The channel of the surface has contained uncoordinated imine nitrogen of bis(pyridyl)-di-imine, in Zn-MOF, which acted as an active base sites for catalytic reaction (Figure 6.9). On the other side, Zn(II) metal ion also acted as a Lewis acid site and activated the carbonyl group by enhancing the electrophilicity. Generally in MOF catalysed reactions, size and shape selectivity along with reactivity of substrates interfere the reaction rate, but in our case, reactivity and size of substrates showed minor effect on the product conversion. Yang et al., reported the Zr(IV)-MOF catalysed Knoevenagel reaction, where decrease in reaction rate was observed upon increasing the

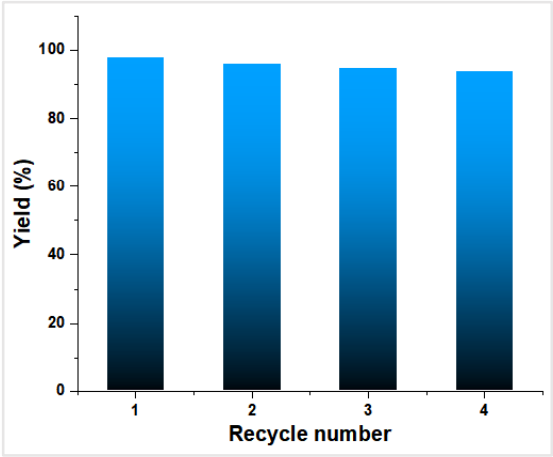

Figure 6.7: Recyclability of **Zn(II)-MOF** catalyst

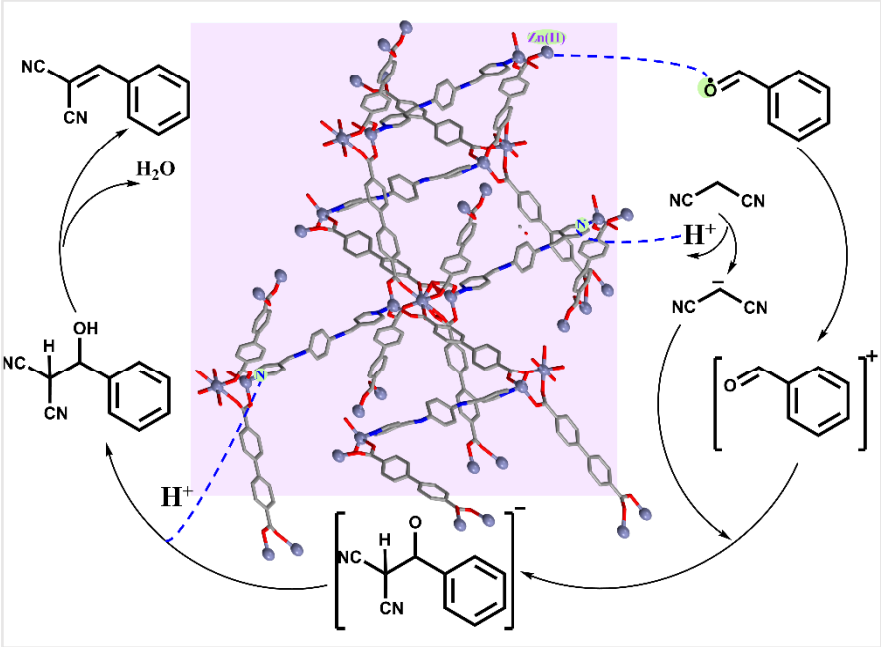

Figure 6.8: Proposed mechanism of Knoevenagel condensation from the catalyst viewpoint

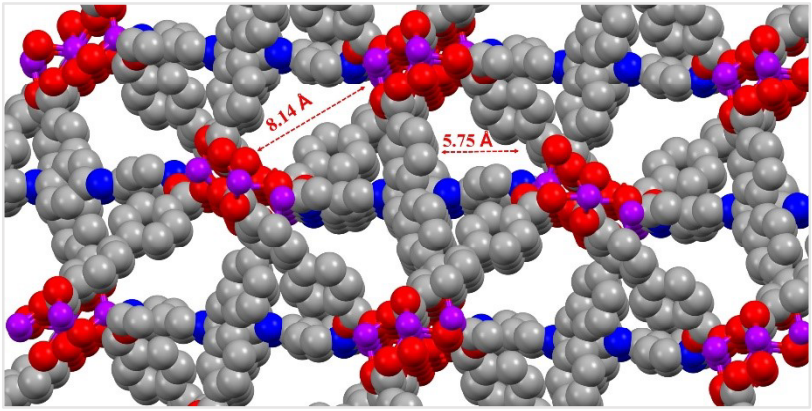

Figure 6.9: Representation of the pores in **Zn-MOF**

dimension of active methylene compound (diethyl malononitrile, ethyl cyanoacetate and tertiary butyl cyanoacetate).[25] The reason for negligible change in the rate of reaction in our case might be use of malononitrile which is having fixed dimension (2.8 × 4.3 $Å^2$).

6.3.5 BET and SEM analysis for pore determination

The Brunauer Emmett Teller (BET) measurement has shown the pore volume of **Zn(II)-MOF** is 0.223 cm^3 g^{-1} and the pore diameter is 44.5 nm (Figure 6.10d). The FE-SEM analysis has resulted in the pore size in the nanometre range (Figure 6.10c). For BET analysis, 33.8 mg of sample was taken. This analysis was performed in the N_2 gas adsorption process followed by the pre-treatment of the sample at 120 °C for 6 hours before the adsorption process. FE-SEM is also helped to identify the structural integrity of the **Zn(II)-MOF** catalyst. The morphology

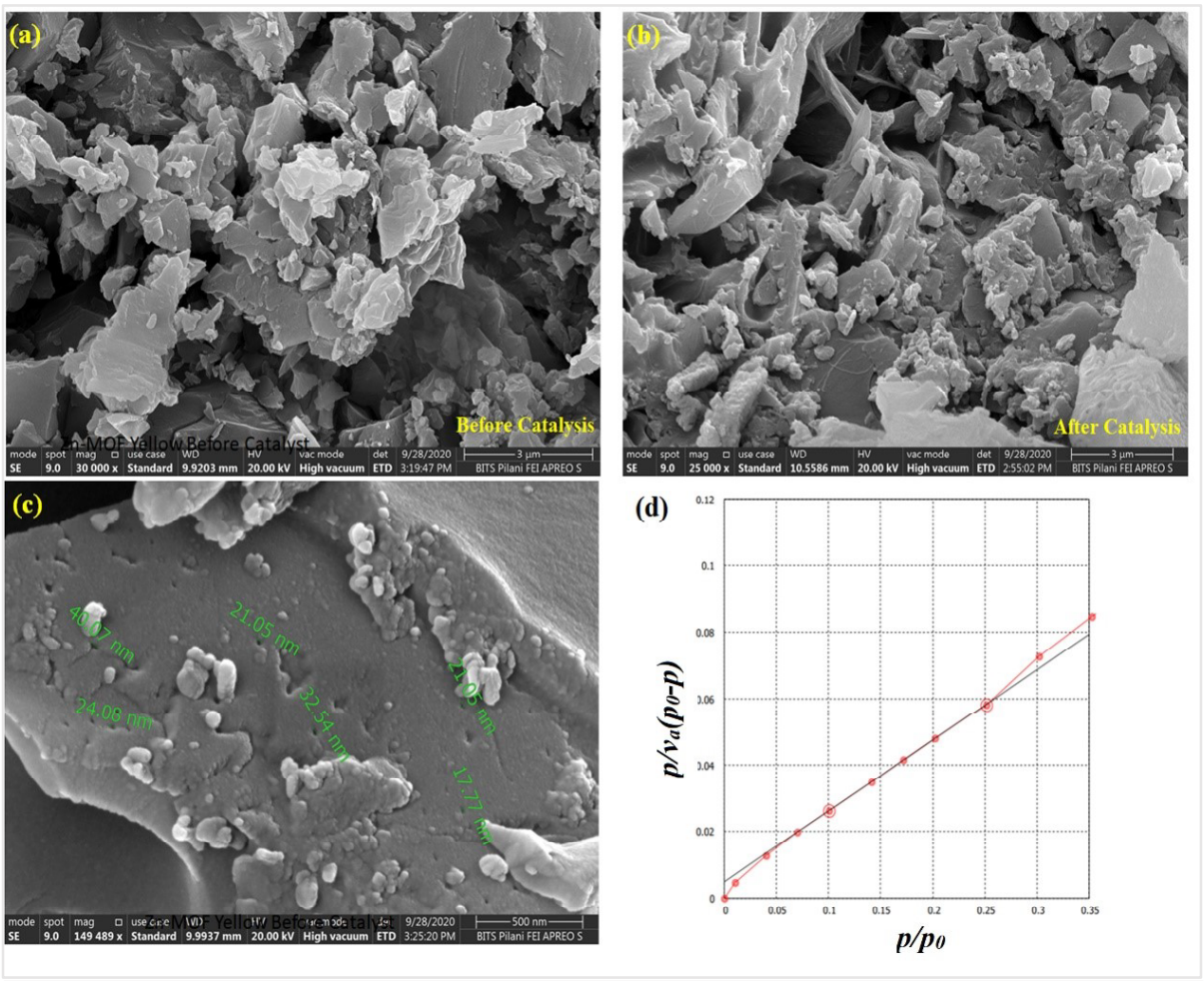

Figure 6.10: SEM results proposed the structural integrity and pore diameter (a), (b) and (c), BET-plot (d)

of **Zn(II)-MOF** is well-matched with the after catalysis of the **Zn(II)-MOF** with particle size 3 μm (Figure 6.10a & b). The narrow pore size has also facilitated the catalyzed reaction.

6.4 Conclusion

A new 3D interpenetrated framework of **Zn(II)-MOF** of pinwheel structure with triangle-and square-tessellated 2D layers was successfully designed using mechanochemically synthesis followed by hydrothermal reaction. Thermally stable **Zn(II)-MOF** was observed acid-base bifunctional catalyst for the Knoevenagel condensation reaction. The derivatives of benzaldehyde were examined with the active methylene compound in methanolic solution by loading of 5 mg of **Zn(II)-MOF** catalyst. The maximum yield of 98% was observed in the benzaldehyde substrate within 30 minutes. The mixed ligand concept MOF synthesis is important for practical application. The rigid bis(pyridyl) imine functionality and dicarboxylate ligand are suitable candidates for the bifunctional MOF catalyst.

6.5 References

[1] Wang C., Liu X., Keser Demir N., Chen J. P., Li K., *Chem. Soc. Rev.,* **2016**, 45(18), 5107-5134.

[2] Gascon J., Corma A., Kapteijn F., Llabrés i Xamena F. X., *ACS Catal.,* **2014**, 4(2), 361-378.

[3] (a) Lee J., Farha O. K., Roberts J., Scheidt K. A., Nguyen S. T., Hupp J. T., *Chem. Soc. Rev.,* **2009**, 38(5), 1450-1459; (b) Hu Z., Zhao D., *CrystEngComm,* **2017**, 19(29), 4066-4081; (c) Remya V. R., Kurian M., *Int. Nano Lett.,* **2019**, 9(1), 17-29; (d) Chughtai A. H., Ahmad N., Younus H. A., Laypkov A., Verpoort F., *Chem. Soc. Rev.,* **2015**, 44(19), 6804-6849; (e) Liu J., Chen L., Cui H., Zhang J., Zhang L., Su C.-Y., *Chem. Soc. Rev.,* **2014**, 43(16), 6011-6061; (f) García-García P., Müller M., Corma A., *Chem. Sci.,* **2014**, 5(8), 2979-3007.

[4] Dhakshinamoorthy A., Opanasenko M., Čejka J., Garcia H., *Adv. Synth. Catal.,* **2013**, 355(2-3), 247-268.

[5] Shi L.-X., Wu C.-D., *Chem. Commun.,* **2011**, 47(10), 2928-2930.

[6] Seo J. S., Whang D., Lee H., Jun S. I., Oh J., Jeon Y. J., Kim K., *Nature,* **2000**, 404(6781), 982-6.

[7] Sabo M., Henschel A., Fröde H., Klemm E., Kaskel S., *J. Mater. Chem.,* **2007**, 17(36), 3827-3832.

[8] Llabrés i Xamena F. X., Abad A., Corma A., Garcia H., *J. Catal.,* **2007**, 250(2), 294-298.

[9] Cho S.-H., Ma B., Nguyen S. T., Hupp J. T., Albrecht-Schmitt T. E., *Chem. Commun.,* **2006**, 2006(24), 2563-2565.

[10] Jiang D., Mallat T., Krumeich F., Baiker A., *J. Catal.,* **2008**, 257(2), 390-395.

[11] Mo K., Yang Y., Cui Y., *J. Am. Chem. Soc.,* **2014**, 136(5), 1746-1749.

[12] Phan N. T. S., Le K. K. A., Phan T. D., *Appl. Catal., A,* **2010**, 382(2), 246-253.

[13] Phan N. T. S., Nguyen T. T., Nguyen C. V., Nguyen T. T., *Appl. Catal., A,* **2013**, 457, 69-77.

[14] Pintado-Sierra M., Rasero-Almansa A. M., Corma A., Iglesias M., Sánchez F., *J. Catal.,* **2013**, 299, 137-145.

[15] Dang T. T., Zhu Y., Ghosh S. C., Chen A., Chai C. L. L., Seayad A. M., *Chem. Commun.,* **2012**, 48(12), 1805-1807.

[16] Song P., Li Y., Li W., He B., Yang J., Li X., *Int. J. Hydrogen Energy,* **2011**, 36(17), 10468-10473.

[17] Park J., Li J.-R., Chen Y.-P., Yu J., Yakovenko A. A., Wang Z. U., Sun L.-B., Balbuena P. B., Zhou H.-C., *Chem. Commun.,* **2012**, 48(80), 9995-9997.

[18] Fujita M., Kwon Y. J., Washizu S., Ogura K., *J. Am. Chem. Soc.,* **1994**, 116(3), 1151-1152.

[19] Alaerts L., Séguin E., Poelman H., Thibault-Starzyk F., Jacobs P. A., De Vos D. E., *Chem. Eur. J.,* **2006**, 12(28), 7353-7363.

[20] Priyadarshini S., Amal Joseph P. J., Kantam M. L., Sreedhar B., *Tetrahedron,* **2013**, 69(31), 6409-6414.

[21] Phan A., Czaja A. U., Gándara F., Knobler C. B., Yaghi O. M., *Inorg. Chem.,* **2011**, 50(16), 7388-7390.

[22] Hartmann M., Fischer M., *Microporous Mesoporous Mater.,* **2012**, 164, 38-43.

[23] Gascon J., Aktay U., Hernandez-Alonso M. D., van Klink G. P. M., Kapteijn F., *J. Catal.,* **2009**, 261(1), 75-87.

[24] Gedrich K., Heitbaum M., Notzon A., Senkovska I., Fröhlich R., Getzschmann J., Mueller U., Glorius F., Kaskel S., *Chem. Eur. J.,* **2011**, 17(7), 2099-2106.

[25] Yang Y., Yao H.-F., Xi F.-G., Gao E.-Q., *J. Mol. Catal. A: Chem.,* **2014**, 390, 198-205.

[26] (a) Miao C., *Inorg. Chem. Commun.,* **2019**, 105, 86-92; (b) Mistry S., Sarkar A., Natarajan S., *Cryst. Growth Des.,* **2019**, 19(2), 747-755; (c) Zhang Y., Wang Y., Liu L., Wei N., Gao M.-L., Zhao D., Han Z.-B., *Inorg. Chem.,* **2018**, 57(4), 2193-2198.

[27] Farrusseng D., Aguado S., Pinel C., *Angew. Chem. Int. Ed.,* **2009**, 48(41), 7502-7513.

[28] Canivet J., Aguado S., Daniel C., Farrusseng D., *ChemCatChem,* **2011**, 3(4), 675-678.

[29] (a) Hwang Y. K., Hong D. Y., Chang J. S., Jhung S. H., Seo Y. K., Kim J., Vimont A., Daturi M., Serre C., Férey G., *Angew. Chem.,* **2008**, 120(22), 4212-4216; (b) Kim S.-N., Yang S.-T., Kim J., Park J.-E., Ahn W.-S., *CrystEngComm,* **2012**, 14(12), 4142-4147.

[30] Juan-Alcañiz J., Ramos-Fernandez E. V., Lafont U., Gascon J., Kapteijn F., *J. Catal.,* **2010**, 269(1), 229-241.

[31] (a) Hasegawa S., Horike S., Matsuda R., Furukawa S., Mochizuki K., Kinoshita Y., Kitagawa S., *J. Am. Chem. Soc.,* **2007**, 129(9), 2607-2614; (b) Sharma M. K., Singh P. P., Bharadwaj P. K., *J. Mol. Catal. A: Chem.,* **2011**, 342-343, 6-10.

[32] Opanasenko M., Shamzhy M., Čejka J., *ChemCatChem,* **2013**, 5(4), 1024-1031.

[33] Kitaura R., Onoyama G., Sakamoto H., Matsuda R., Noro S.-i., Kitagawa S., *Angew. Chem. Int. Ed.,* **2004**, 43(20), 2684-2687.

[34] Masoomi M. Y., Beheshti S., Morsali A., *J. Mater. Chem. A,* **2014**, 2(40), 16863-16866.

[35] Masoomi M. Y., Beheshti S., Morsali A., *Cryst. Growth Des.,* **2015**, 15(5), 2533-2538.

[36] Panchenko V. N., Matrosova M. M., Jeon J., Jun J. W., Timofeeva M. N., Jhung S. H., *J. Catal.,* **2014**, 316, 251-259.